JACS
JOURNAL OF THE AMERICAN CHEMICAL SOCIETY

Article

pubs.acs.org/JACS

Keys for the Existence of Stable Dimers of Bis-tetrathiafulvalene (bis-TTF)-Functionalized Molecular Clips Presenting $[TTF]^{\bullet+}\cdots[TTF]^{\bullet+}$ Long, Multicenter Bonds at Room Temperature

Maria Fumanal,[§] Marçal Capdevila-Cortada,[§] Joel S. Miller,[†] and Juan J. Novoa*[,§]

[§]Departament de Química Física and IQTCUB, Facultat de Química, Universitat de Barcelona, Av. Diagonal 645, 08028 Barcelona Spain

[†]Department of Chemistry, University of Utah, Salt Lake City, Utah 84112-0850, United States

Supporting Information

ABSTRACT: A systematic theoretical and computational investigation is performed to determine the keys governing the existence, in acetonitrile solutions, of dimers of bis-tetrathiafulvalene (bis-TTF)-functionalized diphenylglycoluril molecular clips ($clip_2^{n+}$) that are stable at room temperature for $n \leq 4$. Although the experimental structure of these dimers in solution is unknown, electronic absorption studies suggest that they have $[TTF]^{l+}\cdots[TTF]^{m+}$ interactions that are preserved at room temperature (note that when $l = m = 1$ these interactions become long, multicenter bonds). In good agreement with the interpretation of the experimental spectroscopic data, all $clip_2^{n+}$ dimers whose charge is ≤ 4 present an optimum geometry that, in all cases, has three short interfragment $[TTF]^{l+}\cdots[TTF]^{m+}$ interactions. The computed $\Delta G(298\ K)$ for these optimum structures matches the available experimental data on the stability of these dimers. Such optimum geometry, combined with the zwitterionic character of the electron distribution in monomers and dimers (most of the net positive charge is equally distributed among the TTF groups, while a 1− au charge is located in the central fused five-membered rings) allows the formation of a maximum of two long, multicenter $[TTF]^{\bullet+}\cdots[TTF]^{\bullet+}$ bonds when all TTF groups host a 1+ au of charge, as in $clip_2^{4+}$. However, these long, multicenter bonds alone do not account for the stability of $clip_2^{n+}$ dimers at room temperature. Instead, the studies carried out here trace the origin of their stability to (1) the zwitterionic character of their charge distribution, (2) the proper geometrical shape of the interacting monomers, which allows the intercalation of their arms, thus making possible the simultaneous formation of two short contacts, both involving the positively charged TTF group of one monomer and the negatively charged central ring of the other, (3) the simultaneous presence of three short contacts among the TTF groups in the optimum geometry of the $clip_2^{n+}$ dimers, which become two long, multicenter bonds and one van der Waals interaction when the four TTF groups host a 1+ charge, and (4) the net stabilizing effect of the solvent.

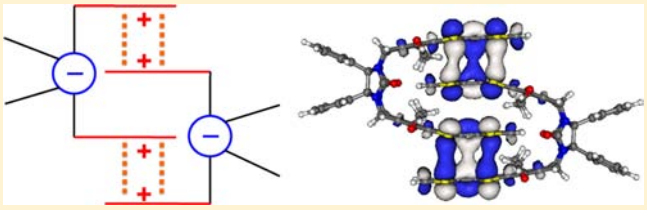

1. INTRODUCTION

The electron donating capabilities of tetrathiafulvalene (TTF) make its mono- and dioxidized forms (i.e., $[TTF]^{\bullet+}$ and $[TTF]^{2+}$) useful building blocks in solids having conducting,[1] superconducting,[2] magnetic,[3] or other physical properties.[4] These oxidized forms are also found in supramolecular host−guest systems that act as sensors[5] or in organic electronics devices, such as organic field-effect transistors (OFETs).[6] However, in some cases the oxidized $[TTF]^{\bullet+}$ can form diamagnetic dimers that are unusable for the aforementioned physical properties. Consequently, a proper understanding of the dimerization processes is desirable in order to control the final physical properties of TTF-based materials.

The nature of the intermolecular interactions between radical ions has been a subject of great interest particularly since the discovery of multicenter, long bonds in their crystals[7,8] and solutions.[7b,9,10] In the solid state, this type of bond was first reported and characterized in salts of reduced tetracyanoethylene (TCNE),[7] where π-$[TCNE]_2^{2-}$ diamagnetic dimers showing interfragment distances substantially shorter than the sum of the van der Waals radii but larger than conventional covalent C−C bonds have been detected (the shortest interfragment distance in π-$[TCNE]_2^{2-}$ dimers is ∼2.9 Å).[7] Subsequently, an increasing number of organic radicals have been reported to have similar dimers with sub-van der Waals intradimer separations. These include, for instance, cyanil[11] and 7,7,8,8-tetracyano-*p*-quinodimethane (TCNQ),[12] neutral radicals, such as phenalenyl and its derivatives,[13] and radical cations, such as tetrathiafulvalene (TTF).[14,15] Additionally, long, multicenter bonding has been reported in zwitterionic π-$[TTF^{\delta+}\cdots TCNE^{\delta-}]$.[16] Kochi and co-workers performed an exhaustive study of the stability of various long bonded dimers in several solvents, among them the π-$[TTF]_2^{2+}$ dimer.[17] The enthalpy and entropy of dimerization of π-$[TTF]_2^{2+}$ in several solvents was estimated: in dichloromethane, these two

Received: June 1, 2013
Published: August 19, 2013

   dx.doi.org/10.1021/ja405352p | J. Am. Chem. Soc. 2013, 135, 13814−13826

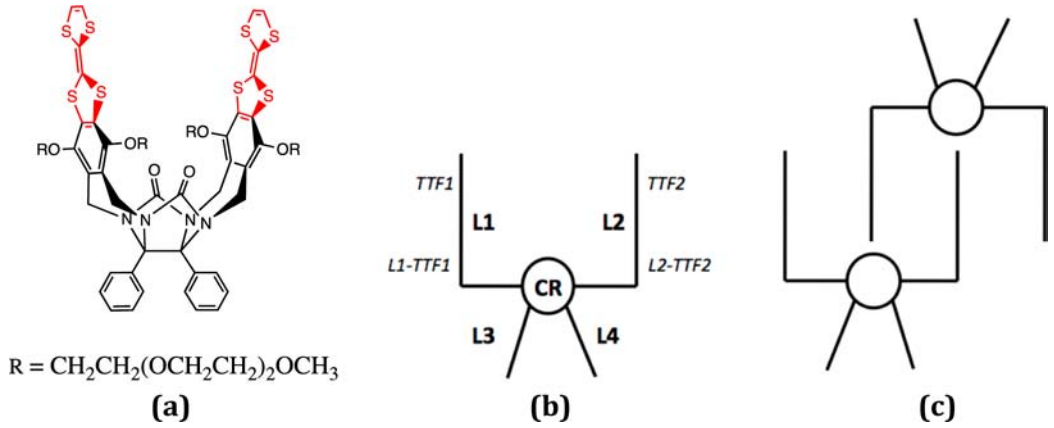

Figure 1. (a) Structure of a bis-TTF-functionalized diphenylglycoluril molecular clip, $clip_1^{n+}$;[25] (b) schematic representation of its structure, where one can observe five constituent groups, (1) central ring (CR) made out of the central fused five-membered rings, (2, 3) the two long arms, pointing upward from the central ring (L1 and L2, each having one TTF group at their end, TTF_i, and a six-membered ring, L_i-TTF_i), and (4, 5) the two short arms, pointing down (L3 and L4); (c) schematic representation of the proposed structure of $clip_2^{n+}$ dimers.[25]

properties become −3.8 kcal mol^{-1} and −18 eu, respectively, while in acetonitrile, their corresponding values are −9.1 kcal mol^{-1} and −31 eu, respectively. The formation of π-$[TTF]_2^{2+}$ dimers in dichloromethane was not observed above −80 °C, while the higher polarity of acetonitrile increased this temperature up to −40 °C.[17]

Previous studies concluded that long, multicenter bonds share all the properties of conventional covalent bonds except their nature, range of stability, and range of equilibrium distance.[7,8,18] Thus, long, multicenter bonded dimers of charged radicals (such as π-$[TCNE]_2^{2-}$ or π-$[TTF]_2^{2+}$) are metastable. From a theoretical perspective, such metastable character arises from the repulsive Coulombic term (E_{el}, caused by their ionic character), which exceeds the sum of the attractive bonding (E_{bond}, due to their radical character) and dispersion energetic terms (E_{disp}), a nonclassical component resulting from the interactions of the instantaneous multipoles produced in both fragments by the motion of the other fragment electrons.[10,19] However, as can already be demonstrated in small $(radical\ ion)_2counterion_2$, aggregates, long, multicenter bonds between charged radicals are formed in the solid state whenever the sum of the attractive (radical ion)···counterion interactions overcomes the repulsion between the radical ions participating in the long bond, plus the repulsion between the two counterions.[10,14,19] Likewise, in solution, long bonds are stabilized because the sum of the (radical ion)···solvent interactions and solvent···solvent interactions exceeds the repulsion between the radical ions involved in the long bond.

Some oxidized [TTF-functionalized] species form stable $[TTF\text{-}functionalized]_2^{2+}$ dimers at room temperature. This behavior has been reported for four families of compounds: (a) $[TTF\text{-}functionalized]_2^{2+}$ dimers included in charged [3]-catenane interlocked rings,[20] whose special experimental properties have been explained on the basis of long bonds after doing an exhaustive theoretical study;[20,21] (b) π-$[TTF]_2^{2+}$ included within the cavity of a cucurbit[8]uril, CB[8][22] (note, in passing, that dimers of methylviologen included in CB[8] are also stable at room temperature);[23] (c) doubly substituted calixarenes;[24] (d) acetonitrile solutions of bis-TTF-functionalized diphenylglycoluril molecular clips[25] whose dimers in solution are presumed to have sub-van deer Waals $[TTF]^{\bullet+}$··· $[TTF]^{\bullet+}$ interactions at room temperature, for reasons not yet fully understood.

Here, we focus our attention on the last type of case, trying to rationalize its experimental behavior. Bis-TTF-functionalized diphenylglycoluril molecular clips ($clip_1^{n+}$) are rigid structures that can be viewed as a central rigid core (the fused five-membered rings) to which two adjacent long arms and two adjacent short arms are attached, the two long arms pointing in opposite direction relative to the short arms (Figure 1). Each long arm has one TTF group attached at its end, which does not interact with the TTF group of the other arm, and a lateral -OR group (R = $CH_2CH_2(OCH_2CH_2)_2OCH_3$) that increases the solubility of the molecular clip. Initially, bis-TTF-functionalized clips are obtained as neutral monomers, $clip_1^0$. However, as in isolated TTF molecules, each TTF group $clip_1^0$ can be oxidized up to a maximum of 4+ per molecular clip (a maximum value of 2+ per group, that is, up to $clip_1^{4+}$). Voltammetric techniques allow the controlled formation of all oxidized monomers, whose positive charge is presumably delocalized over the noninteracting TTF groups. Mass spectroscopy studies[25] indicated the presence of $clip_2^{n+}$ dimers stable at room temperature for $0 < n \leq 4$. Since the UV spectrum of these stable $clip_2^{n+}$ dimers finds the characteristic features of short $[TTF]^{\bullet+}\cdots[TTF]^{\bullet+}$ long, multicenter bonds, even at room temperature, the structure in Figure 1c[25] was proposed. However, a full rationalization of their structure and all the other experimental results, based on sounding theoretical studies, has never been done.

The present work provides a rationalization of the experimental properties of bis-TTF-functionalized diphenylglycoluril molecular clips, based on exhaustive M06L computations on all $clip_1^{m+}$ (m = 0−4) monomers and $clip_2^{n+}$ (n = 0, 1, 2, 3, 4, 6, or 8) dimers. The n = 6 and n = 8 dimers were taken as representative of the behavior of $n > 4$ dimers. For each $clip_2^{n+}$ dimer, its optimum geometry was computed and the resulting structure was analyzed focusing on the existence of short [TTF]···[TTF] contacts between its two monomeric fragments. Additionally, the stability of $clip_2^{n+}$ with respect to dissociation into $clip_1^{l+}$ and $clip_1^{m+}$ (the sum of the monomer charge is equal to that for the dimer, that is, $n = l + m$) was also evaluated. The electronic structure and charge distribution of $clip_1^{m+}$ and $clip_2^{n+}$ was also computed. These studies were first performed on isolated dimers and then on dimers dissolved in

dx.doi.org/10.1021/ja405352p | J. Am. Chem. Soc. 2013, 135, 13814−13826

acetonitrile. Finally, the nature of the interaction energy was analyzed in order to determine the origin of the room temperature stability of the $clip_2^{n+}$ (n = 0−4) dimers in acetonitrile solutions. These studies had three final aims: (a) determining the key features that govern the self-association of $clip_2^{n+}$ dimers and how they vary with the dimer net charge; (b) finding how many, if any, sub-van der Waals $[TTF]^{l+}\cdots[TTF]^{m+}$ contacts are long, multicenter bonds; (c) comparing the bond energy of the long, multicenter $[TTF]^{\bullet+}\cdots[TTF]^{\bullet+}$ bond formed in $clip_2^{4+}$ with that found in the π-$[TTF]_2^{2+}$ dimer and finding the reasons for the room temperature stability of $clip_2^{n+}$, $n \leq 4$. These findings are needed for a better understanding of the $[TTF]^{\bullet+}$ dimerization, as well as to improve the current understanding of the properties of long, multicenter $[TTF]^{\bullet+}\cdots[TTF]^{\bullet+}$ bonds. They also provide an in depth quantitative knowledge of the self-association of diphenylglycoluril molecular clips, here systematically studied as a function of the monomer oxidation state. To the best of our knowledge, this is the first time that an exhaustive study of this kind is reported.

2. METHODOLOGICAL DETAILS

Previous studies on π-$[TTF]_2^{2+}$ dimers in solution[15] concluded that the presence of $[TTF]^{\bullet+}\cdots[TTF]^{\bullet+}$ long, multicenter bonds in solution and all their known physical properties can be properly described by π-$[TTF]_2^{2+}(solvent)_m$ aggregates, m being a reasonably small value that allows the inclusion of the dominant energetic components of the π-$[TTF]_2^{2+}$ dimer first solvation shell. Recent work on functionalized π-$[TTF]_2^{2+}$ dimers[21] demonstrated that the PCM continuous solvent model[26] completely reproduces the stability in solution of these dimers, their optimum geometry, and the presence of long, multicenter bonds. Therefore, the PCM method was chosen in this work for the studies in solution. In none of the previous studies were counterions included in the model aggregates. Furthermore, experimental evidence[27] indicates that counterion-containing aggregates are not usually formed in solution at the concentration range employed in the π-$[TTF]_2^{2+}$ and $clip_2^{n+}$ experimental studies.[17,25]

The computational study of the properties of the dimers of bis-TTF-functionalized diphenylglycoluril molecular clips is carried out hereafter in four consecutive steps. First of all, the optimum geometry and the ground state electronic structure of isolated $clip_1^{m+}$ (m = 0−4) monomers are computed and analyzed, in order to gain insight into the nature of the $clip_1^{l+}\cdots clip_1^{m+}$ interaction. Such information is used to guide the search for the optimum geometry of the isolated $clip_2^{n+}$ (n = 0, 1, 2, 3, 4, 6, or 8) dimers, at their electronic ground state, carried out in the second step. In the third step, the optimum structure of isolated $clip_1^{m+}$ and $clip_2^{n+}$ computed before is reoptimized using the PCM continuous model,[26] thus accounting for the solvent effects. Finally, in the fourth and last step, in order to determine the origin of the room temperature stability of the $clip_2^{n+}$ (n = 0−4) dimers in acetonitrile solutions, an energy partition analysis of the interaction energy of these dimers is carried out.

All energy computations were performed (on their electronic ground state) using the M06L density functional[28] and the 6-31G(d,p) basis set.[29] The use of a pure meta-GGA functional reduces significantly the computational cost compared with a hybrid functional (such as M06-2X), with only a tiny loss of accuracy in geometries and energies.[30] The M06L functional was chosen because (a) recent work has demonstrated its reliability on large nonbonded molecular complexes,[30] (b) its ability to reproduce the experimental results on supramolecular functionalized-TTF systems has been proven,[20a,21] and (c) tests carried out in this work (see below) show that it reproduces the interaction energy of isolated π-$[TTF]_2^{n+}$ (n = 0−4) dimers obtained in extensive high-level RASPT2[31,32] computations. These RASPT2 calculations were done using a (28 − n, 2, 2; 11, 4, 5)[33] restricted active space, n being the charge on the dimer. Such space is based on a (28 − n, 20) complete active space that results from extrapolating those employed in previous $[TTF]^0$ and $[TTF]^{\bullet+}$ calculations.[34]

Interaction energies have their basis set superposition error (BSSE) corrected according to the counterpoise method.[35,36] In order to facilitate these computations, in all monomers and dimers, the two lateral OR groups (R = $CH_2CH_2(OCH_2CH_2)_2OCH_3$, see Figure 1), experimentally used only to improve solubility, were substituted by methoxy groups.

The reliability of the 6-31G(d,p) basis set results against the addition of diffuse functions was tested by comparing the optimum geometry and electronic structure obtained using the 6-31G(d,p), 6-31+G(d,p), and 6-31++G(d,p) basis sets for two representative systems, $clip_1^{2+}$ and $clip_2^{4+}$. The results for the basis with and without diffuse functions are almost identical (see Figure S1 and Tables S1−S3, Supporting Information), thus validating the general use of the 6-31G(d,p) basis set.

All energetic calculations were done using the appropriate options in the Gaussian09 suite of programs,[37] except the RASPT2 calculations, for which Molcas7.6 was used.[38]

3. RESULTS AND DISCUSSION

3.1. Electronic Structure and Optimum Geometry of Isolated $clip_1^{n+}$ (n = 0−4) Monomers. *3.1.1. The Electronic Structure and Geometry of the Neutral $clip_1^0$ Monomer.* At the M06L/6-31G(d,p) level, the electronic ground state of the $clip_1^0$ monomer is a closed-shell singlet well below the energy of the lowest energy open-shell singlet and triplet states. Geometry optimization of the isolated $clip_1^0$ monomer in its singlet ground state leads to the V-shaped structure shown in Figure 2. In this optimum geometry each TTF has a boat-like

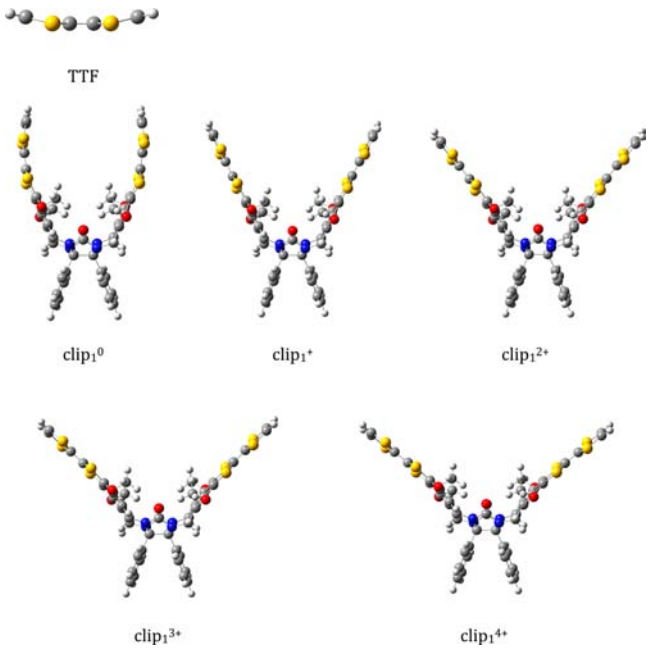

Figure 2. Optimum geometries of the neutral TTF molecule and the $clip_1^{n+}$ (n = 0−4) monomers computed at the M06L/6-31G(d,p) level.

conformation, similar to that found at the optimum structure of an isolated TTF molecule (Figure 2). The shortest distance between the two TTF groups in $clip_1^0$ is 7.7 Å, while the angle between the two long arms is 68.4° (Table 1; see Figure S2, Supporting Information, for the geometrical parameters definition).

A first hint about the main features of the electronic structure of $clip_1^0$ in its singlet ground state is obtained from examining

dx.doi.org/10.1021/ja405352p | J. Am. Chem. Soc. 2013, 135, 13814−13826

Table 1. Values of the Shortest TTF···TTF Distance (r), Angle (α), and Dipole Moment (μ) of clip$_1^{n+}$ (n = 0−4) Monomers, Both Computed Isolated and in Acetonitrile Solution, Using the PCM Model[a]

	r (Å)		α (deg)		μ (D)	
	isolated	solution	isolated	solution	isolated	solution
clip$_1^0$	7.7	7.8	68.4	69.8	1.5	1.6
clip$_1^+$	8.0	7.8	75.4	72.0	10.4	14.3
clip$_1^{2+}$	8.6	7.9	85.3	74.4	20.5	29.3
clip$_1^{3+}$	9.1	8.3	93.1	80.6	24.4	42.5
clip$_1^{4+}$	9.5	8.3	99.6	81.0	26.2	55.1

[a]Both distance and angle are defined in Figure S2, Supporting Information. M06L/6-31G(d,p) calculations.

the net charge on the five parts in which one can naturally divide the monomer: the central ring (CR), its two long arms, L1 and L2 (each hosting a TTF group at their end), and its two short arms, L3 and L4 (Figure 1b). The net charge on each part was computed by adding the atomic charge of each of their atoms, obtained from a Mulliken population analysis of the ground state wave function (as shown in Figure S3, Supporting Information; other population analyses provide a nearly identical charge distribution). The most remarkable feature of the ground state electronic distribution is its zwitterionic character:[39] the CR hosts a 1− atomic unit (au) net charge, each L1 and L2 long arms has a net 0.4+ au charge, and each short arm has 0.1+ au charge (Figure 3). Such zwitterionic

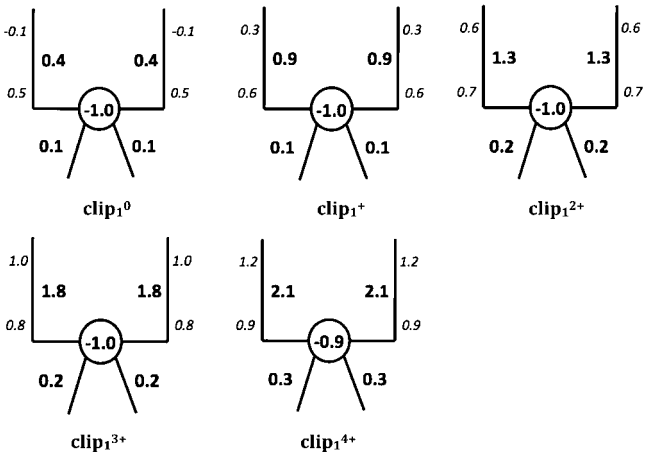

Figure 3. Representation of the net charge distribution on clip$_1^{n+}$ (n = 0−4) monomers studied in this work. For each monomer, the net atomic charge in the five groups defined in Figure 1 is given, indicating in italics the charge in the TTF$_i$ and L$_i$-TTF$_i$ parts of the L$_i$ arms. The net charge in each group is computed by adding the Mulliken atomic charges for all atoms of the group.

nature of the isolated clip$_1^0$ is consistent with the computed dipole moment (1.5 D), similar to that for an isolated water molecule.[40] The presence of such large charge shift from L1 and L2 to CR is only possible if the orbitals in CR are much more stable than those in L1 and L2. This results in a CR−L$_i$ bonding orbital dominated by the CR orbitals, for both L1 and L2. Such energy mismatch also makes the through-bond L1−CR−L2 interaction very small. Since the two TTF groups are also too far away to allow any non-negligible overlap of their orbitals (and therefore any through-space interaction), the two TTF groups behave as nearly independent.

The MO structure of clip$_1^0$ is consistent with the aforementioned zwitterionic electronic distribution and the near independence of the two TTF groups of an isolated clip$_1^0$ monomer. At the M06L level, clip$_1^0$ has two nearly degenerate HOMOs (labeled as MO1 and MO2 in Figure 4), each one almost entirely localized on one terminal TTF group. Both orbitals have the same shape as the HOMO of an isolated [TTF] neutral molecule (Figure 4).

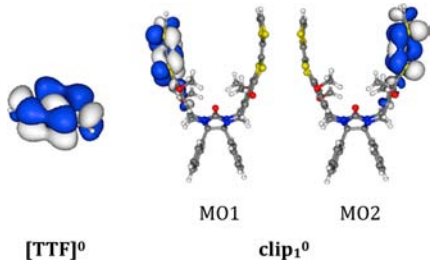

Figure 4. Shape of the highest two MOs of clip$_1^0$. The orbitals have been computed for the monomer ground state (M06L/6-31G(d,p) calculations) at its optimum geometry. The HOMO of the neutral [TTF] is also plotted, for comparison.

3.1.2. The Electronic Structure and Geometry of the clip$_1^+$ to clip$_1^{4+}$ Charged Monomers. Cationic clip$_1^+$ to clip$_1^{4+}$ monomers are obtained by successive oxidations of clip$_1^0$. Therefore, in a first approach, one can expect that the four electrons removed in these processes are those placed in the two nearly doubly degenerate HOMO orbitals of clip$_1^0$, because they are the highest ones in energy. The validity of this statement along each oxidation step is checked by doing M06L/6-3G(d,p) calculations.

The ground electronic state of clip$_1^+$, according to M06L/6-31G(d,p) calculations, is the doublet that results from extracting one electron from one nearly doubly degenerate HOMO orbital in clip$_1^0$ (Figure S4, Supporting Information). The optimum geometry optimization of clip$_1^+$ in its ground state also has a V-shaped structure (Figure 2), the angle between its two long arms being 7° larger than that in clip$_1^0$. As a result, the shortest distance between the TTF groups increases up to 8.0 Å (Table 1). Its electronic structure has its only unpaired electron equally delocalized over both TTF units (rather than fully localized on only one of the TTF groups), consistent with its symmetric optimum geometry and charge distribution (Figure 3). Its charge distribution is also zwitterionic, with 1− au located in the CR part, 0.1+ au in each short arm, and 0.9+ au in each long arm. By comparing such charge distribution with that for the neutral monomer, one finds that the 1+ au net charge hosted by clip$_1^+$ is mostly stored in the long arms: each one increases their charge by 0.4+ au (each TTF group with a 0.3+ au, while 0.1+ au goes to its attached six-membered rings). Consequently, clip$_1^+$ has a stronger zwitterionic character than clip$_1^0$, naturally reflected in a larger dipole moment (10.4 D in clip$_1^+$ compared with 1.5 D in clip$_1^0$).

Formally, when two electrons are removed from clip$_1^0$ to produce clip$_1^{2+}$, they could come from the same TTF group (therefore, formally creating a (2+,0) charge distribution on the two TTF groups) or from a different TTF group (thus ending in a (1+,1+) distribution). One expects that a (2+,0) distribution would result in a closed-shell singlet state while the (1+,1+) distribution, with one unpaired electron on each

dx.doi.org/10.1021/ja405352p | J. Am. Chem. Soc. 2013, 135, 13814−13826

nearly independent TTF group, would result in an open-shell singlet or a triplet ground state (keep in mind that the two TTF groups of the same monomer are too far away to allow the formation of an intramolecular long, multicenter bond, which would result in a closed-shell state). Between these two options, M06L/6-31G(d,p) calculations indicate that the open-shell singlet is the ground state, while the triplet state is just 0.1 kcal/mol higher. Thus, $clip_1^{2+}$ is a diradical with one electron located in each TTF group (Figure S4, Supporting Information), consistent with the computed spin distribution (Figure 5). At

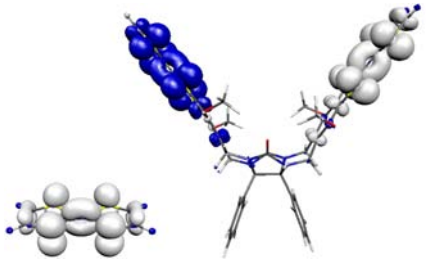

Figure 5. Spin distribution of isolated $[TTF]^{\bullet+}$ cation (left) and $clip_1^{2+}$ dication (right) at their ground state.

room temperature, the singlet and triplet states will be equally populated and paramagnetic behavior should be observed. The $clip_1^{2+}$ charge distribution, Figure 3, is also zwitterionic, with a net 1− au charge in the CR group, 0.2+ au in each short arm, and 1.3+ au in each long arm (0.6+ au in its TTF group and 0.7+ au in the attached six-membered ring). Therefore, the long arms host the 2+ au formal charge from the oxidation, plus some extra charge that results from the charge shift, due to the higher stability of the CR orbitals with respect to the long arms orbitals. This increase in the zwitterionic character is consistent with the increase in the dipole moment to 20.5 D. It also explains the increase in the separation between the two $[TTF]^{\bullet+}$ groups observed for the open-shell singlet ground state of $clip_1^{2+}$ at its optimum geometry (Table 1, Figure 2).

The ground states of $clip_1^{3+}$ and $clip_1^{4+}$ are a doublet and a closed-shell singlet, respectively, consistent with a further decrease in the electron occupation of the nearly double-degenerate HOMOs of $clip_1^{0}$ (Figure S4, Supporting Information). The electronic structure of the two fragments are also zwitterionic, with a 1− au charge located on the central CR group and 1.7+ and 2.1+ au located in the two long arms, mostly over the TTF groups (Figure 3). As a consequence, the dipole moment becomes even larger (24.4 D in $clip_1^{3+}$ and 26.2 D in $clip_1^{4+}$). The optimum geometry of isolated $clip_1^{3+}$ and $clip_1^{4+}$ monomers at their ground state, Figure 2, is also V-shaped, the shortest distance between the TTF groups also being larger (9.1 and 9.5 Å, respectively). Note the correlation between the increment of net charge on the TTF groups and the increase in the angle between the two long arms (and, as a result, the larger distance between the TTF groups).

3.2. Electronic Structure and Optimum Geometry of Isolated $clip_2^{n+}$ (n = 0, 1, 2, 3, 4, 6, or 8) Dimers. An identification of the most stable geometry of the $clip_2^{n+}$ dimers requires a preliminary analysis of the isolated $clip_1^{l+}\cdots clip_1^{m+}$ interaction aimed at qualitatively predicting, among all likely minimum energy structures, the most plausible orientation of the absolute minimum. Such a task was achieved in three steps. In the first one, the nature of the $clip_1^{l+}\cdots clip_1^{m+}$ intermolecular interactions was determined. Such information allowed the identification, on qualitative grounds, of the most probable orientation of the absolute minimum as a second step. Then, in the third step, the most stable structure was optimized and analyzed for each isolated $clip_2^{n+}$ dimer.

3.2.1. The Nature of $clip_1^{l+}\cdots clip_1^{m+}$ Intermolecular Interactions. The nature of any intermolecular interaction can be determined by finding the dominant energetic component in an IMPT[41] perturbative calculation of the interaction energy. This method can also be used to obtain qualitative information about the nature of the interaction energy, by analyzing the properties of the dominant component of the interaction energy via the IMPT scheme.[42]

Assuming, as is commonly found, that the polarization (E_{pol}) and charge-transfer (E_{ct}) components of the IMPT interaction energy are 1 order of magnitude smaller than the remaining ones,[42] the IMPT intermolecular interaction energy between two open shell fragments, A and B, takes the following expression:[13c]

$$E_{int} \approx E_{er} + E_{el} + E_{disp} + E_{bond} \quad (1)$$

where each term has the following physical meaning: (1) E_{er} is the exchange−repulsion energetic component that is always energetically repulsive due to the repulsion that electrons feel when they occupy the same point of the space, in accord with the Pauli exclusion principle (this term is known to be proportional to the exponential of the overlap integral between the A and B wave functions); (2) E_{el} is the electrostatic energetic component of the nonpolarized system, which can be accurately approximated as a sum of classical multipoles (i.e., the sum of the charge−charge, charge−dipole, dipole−dipole, etc. components; when the smaller polarization component, E_{pol}, is added, one obtains the true electrostatic energy); (3) E_{disp} is the dispersion energetic component, a nonclassical term that arises from the instantaneous dipole−dipole interactions resulting from the correlated motions of the electrons in A and B; (4) E_{bond} is the bonding energetic component, associated with the pairing, produced in the dimer, of the unpaired electrons of fragments A and B. Because E_{er} is always energetically repulsive, the remaining three terms (E_{el}, E_{disp}, and E_{bond}) are the only ones to be analyzed when one looks for stable geometries of an AB complex.

One can now apply these ideas to the analysis of the $clip_1^{l+}\cdots clip_1^{m+}$ interactions. Previous evidence indicates that E_{el} dominates whenever the interacting fragments are charged or have a strong dipole moment, as is the case in all $clip_1^{m+}$ (m = 0−4) monomers.[43] The most stable orientation of two dipoles is found when they are in an antiparallel disposition. The three orientations shown in Figure 6 fulfill such a criterion and, consequently, are good initial candidates to locate the most stable orientation of $clip_2^{n+}$ dimers. Among them, that in Figure 6c also maximizes E_{disp}, due to the presence of short-distance interactions between the lone-pair electrons of the TTF groups, whatever the dimer net charge. Finally, E_{bond} can only be present whenever the two interacting monomers have unpaired electrons and their SOMOs present non-negligible overlap. As discussed above, $clip_1^{+}$, $clip_1^{2+}$, and $clip_1^{3+}$ have unpaired electrons, mostly located on the TTF groups (0.5, 1.0, and 1.5 electrons on each TTF, respectively). Furthermore, charged $clip_2^{n+}$ dimers oriented as in Figure 6c allow the formation of three short-distance intermolecular TTF···TTF contacts that interconnect the four TTF groups. When the two TTF groups of these short-distance TTF···TTF contacts host one unpaired electron, as in $clip_1^{2+}$, these become long, multicenter bonds, a

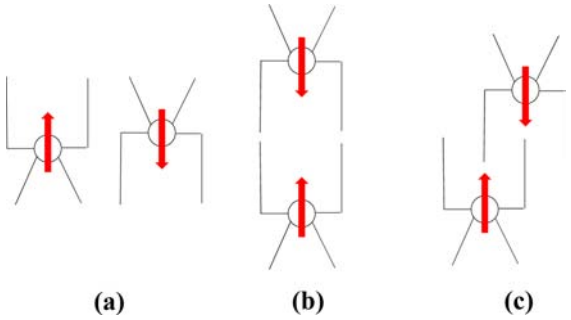

Figure 6. Three possible geometrical dispositions of the $clip_1^{n+}\cdots clip_1^{m+}$ dimers, which are reasonable candidates for their most stable orientation.

fact that affects the value of E_{bond}. A maximum of two of long, multicenter bonds can be formed in $clip_2^{4+}$ dimers, by pairing the unpaired electrons among the four $[TTF]^{\bullet+}$ groups. This situation is experimentally detected in its UV−vis spectrum.[25]

Using the same reasoning, the $clip_2^{6+}$ dimer can be described as a $clip_1^{3+}\cdots clip_1^{3+}$ interaction. If one accepts that $clip_1^{3+}$ monomers distribute their 3+ charge following a (2+,1+) distribution, while the other follows a (1+,2+) distribution, one long, multicenter bond could be formed in the central short TTF···TTF contact, where the two $[TTF]^{\bullet+}$ groups would be located. However, the bonding in $clip_2^{6+}$ is not so simple, because there are other ways of arranging two (2+,1+) distributions, besides the fact that (1.5+,1.5+) distributions are also possible. A similar complex situation is faced in $clip_2^{2+}$, formally a $clip_1^{+}\cdots clip_1^{+}$ interaction. Now both monomers could present a (1+,0) or (0.5+,0.5+) charge distribution, although the presence of long multicenter bonds has not been experimentally detected in $clip_2^{2+}$.[44] The intermolecular bonding in $clip_2^{+}$, $clip_2^{3+}$, $clip_2^{5+}$, and $clip_2^{7+}$ is also a complex matter, while $clip_2^{0}$ and $clip_2^{8+}$ have no long, multicenter bonds because they have no unpaired electrons. Given the complex nature of the intermolecular bonding in all clips with net charge different than 4, they will be subject of a further specific study.

3.2.2. Optimum Geometry and Relative Stability of the $clip_2^{n+}$ (n = 0, 1, 2, 3, 4, 6, or 8) Dimers. The most stable geometry of $clip_2^{0}$ was computed at the M06L/6-31G(d,p) level starting from a reasonable guess of Figure 6c configuration. For all other dimers, the $clip_2^{n+}$ M06L/6-31G(d,p) geometry optimization started from the optimum geometry of $clip_2^{(n-1)+}$. The study also includes $clip_2^{6+}$ and $clip_2^{8+}$, as representatives of the properties of $clip_2^{n+}$ (n = 5−8) dimers, aiming at determining why they are not experimentally observed at room temperature.

The optimum geometry obtained for each isolated $clip_2^{n+}$ (n = 0, 1, 2, 3, 4, or 6) dimer in their electronic ground state, along with its ground state spin multiplicity, is shown in Figure 7. The geometry of $clip_2^{8+}$ is not shown, since it dissociates into its two $clip_1^{4+}$ monomers. As shown in Figure 7, all minimum energy structures, besides $clip_2^{6+}$, preserve the starting Figure 6c configuration (a more detailed analysis of their similarities can be done by looking at Table S4, Supporting Information, where the most relevant interfragment parameters, defined in Figure S5, Supporting Information, have been collected).[45] The BSSE-uncorrected and corrected interaction energies, as well as their formation energies, of all dimers at their optimum geometry (for $clip_2^{8+}$, at the optimum geometry of $clip_2^{6+}$) are collected in Table 2. According to these formation energies, $clip_2^{0}$, $clip_2^{+}$, and $clip_2^{2+}$ are bound minima stable against their dissociation

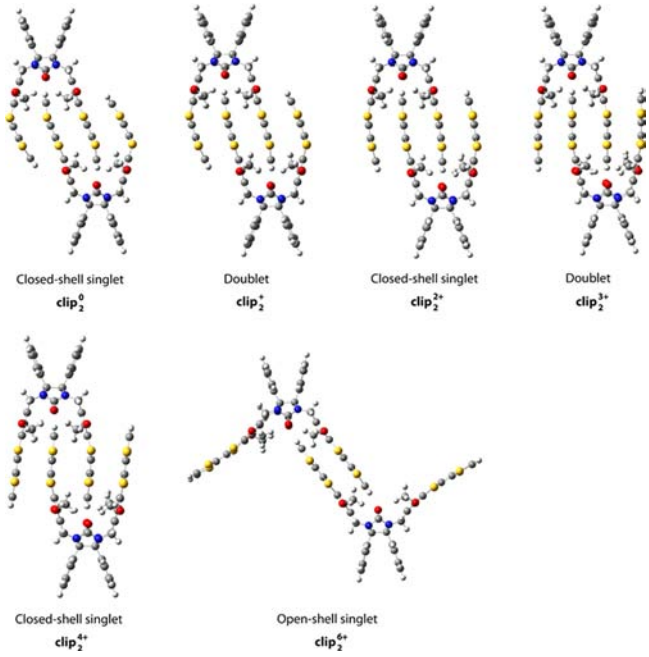

Figure 7. Optimum geometries of isolated $clip_2^{n+}$ dimers (n = 0, 1, 2, 3, 4, or 6) in their ground electronic state (shown under each geometry). The optimum structure of $clip_2^{8+}$ is not shown because it dissociates into its two monomers.

into two monomers, while $clip_2^{3+}$, $clip_2^{4+}$, and $clip_2^{6+}$ are metastable minima.[46] A similar trend is observed when the free energies of formation at 298 K are considered (Table 2). The main difference with respect to formation energy values is that $clip_2^{2+}$ is unstable against dissociation. These results fail to satisfy the available experimental information, thus suggesting that solvent effects could be relevant (vide infra).

In all dimers, the charge distribution in both fragments is similar to that found in their corresponding monomers. This is graphically demonstrated in Figure 8, where the charge localized in each of the five parts defined on the monomers (Figure 1b) is analyzed for the two fragments of each dimer. Therefore, each fragment of a dimer preserves its zwitterionic electronic structure, which creates an important dipole moment. Consistent with such electron distribution, the shape of the highest four occupied orbitals of $clip_2^{0}$ (Figure 9) are the bonding and antibonding combinations of the two nearly degenerate HOMOs of $clip_1^{0}$. These four orbitals should have the eight electrons involved in the eight steps of the $clip_2^{0}$ to $clip_2^{8+}$ oxidations. As shown in Figure 9 (left), this is only the case in the oxidations from $clip_2^{0}$, $clip_2^{+}$, and $clip_2^{2+}$. Beyond $clip_2^{3+}$, the orbitals located in the L3 and L4 short arms become less stable than those located in the L1 and L2 long arms. This explains the increase of charge found in the short arms of $clip_2^{8+}$.

3.3. Solvent Effects: Structure and Stability of the $clip_1^{m+}$ and $clip_2^{n+}$ in Acetonitrile Solutions. All available experimental data on the stability of $clip_2^{n+}$ dimers obtained in acetonitrile solution[25] disagree with the free energies of formation computed on isolated dimers (Table 2). Given the ionic character of these dimers, this disagreement could result from solvent effects. Hereafter, the impact of these effects on the free energy of formation of $clip_2^{n+}$ dimers is accurately evaluated using the PCM continuous solvation model.

dx.doi.org/10.1021/ja405352p | J. Am. Chem. Soc. 2013, 135, 13814−13826

Table 2. Interaction and Formation Energy[a] for the Optimum Geometry of Isolated $clip_2^{n+}$ (n = 0, 1 2, 3, 4, 6, or 8) Dimers (Figure 7)

	$clip_2^{0}$	$clip_2^{+}$	$clip_2^{2+}$	$clip_2^{3+}$	$clip_2^{4+}$	$clip_2^{6+}$	$clip_2^{8+}$
				Isolated			
E_{int}	−61.3	−75.7	−37.0	−13.8	+70.4	+171.4	+347.7[b]
E_{int}^{CP}	−49.5	−64.2	−25.5	−2.7	+80.9	+197.1	+378.2[b]
E_{for}	−50.8	−61.9	−23.0	+12.1	+98.6	+207.1	+385.9[b]
E_{for}^{CP}	−39.0	−50.3	−11.3	+23.4	+109.1	+232.9	+416.4[b]
ΔG (298 K)	−19.1	−31.0	+8.2	+42.0	+123.9	+238.9	[c]
				In Acetonitrile Solutions			
E_{for}	−45.9	−52.8	−52.6	−50.7	−41.2	−16.5	+0.8
ΔG (298 K)	−12.2	−20.7	−20.6	−18.1	−9.5	+16.9	+29.5

[a]Obtained at M06L/6-31G(d,p) level, with and without counterpoise correction. Energy values in kcal/mol. [b]Estimation made at the optimum geometry of the $clip_2^{6+}$ dimer. [c]It is not a minimum in the potential energy surface of the system.

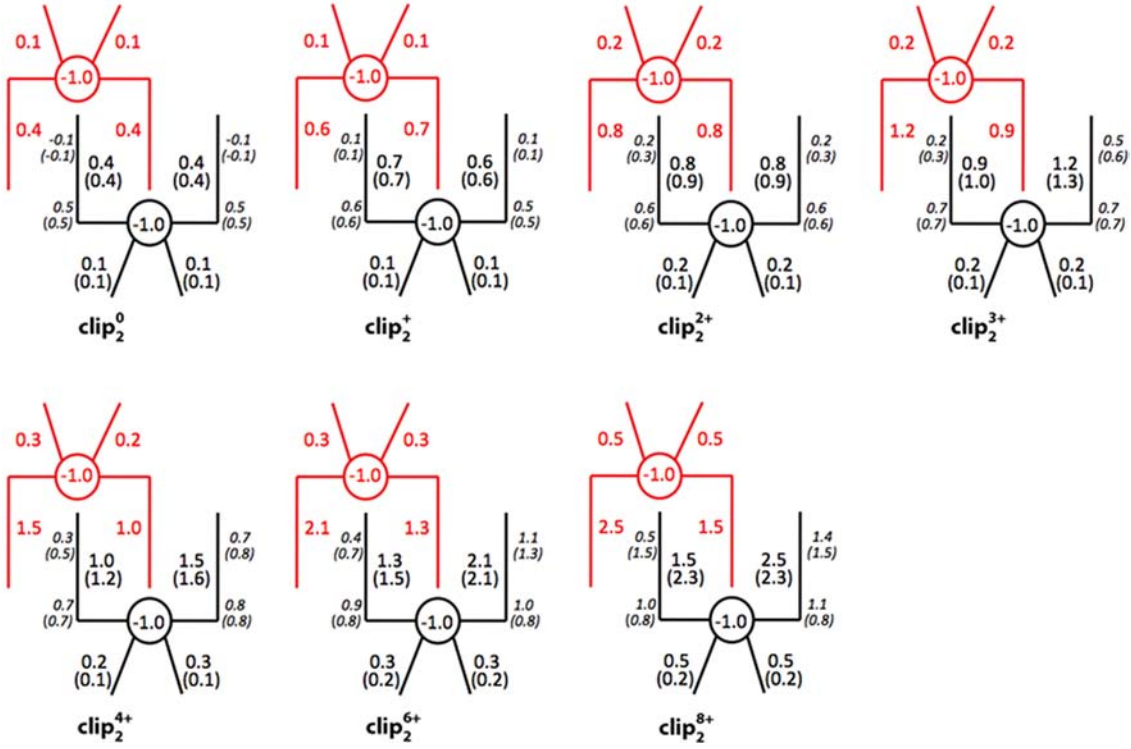

Figure 8. Representation of net charge distribution on the isolated $clip_2^{n+}$ (n = 0, 1, 2, 3, 4, 6, or 8) dimers studied in this work. Charge values in acetonitrile solution are given within parentheses (since the distribution is symmetrical, they are only specified over one monomer to facilitate comprehension). The computations have been done at their optimum geometry (except in isolated n = 8, which was obtained at the optimum geometry of isolated $clip_2^{6+}$). In each monomeric fragment of the dimers, the net atomic charge in the five groups defined in Figure 1 is given, indicating in italics the charge in the TTF_i and L_i-TTF_i parts of the L_i arms. The net charge in each group is computed by adding the Mulliken atomic charges for all atoms of the group.

3.3.1. Solvent Effects on the $clip_1^{m+}$ Properties. With the PCM model, the optimum structures of $clip_1^{m+}$ were first reoptimized at the M06L/6-31G(d,p) level starting from their isolated structure. The optimum geometries of $clip_1^{0}$ to $clip_1^{4+}$ monomers in acetonitrile are similar to their optimum isolated geometries, Figure S6, Supporting Information, the main difference being the smaller angle between the two long arms in acetonitrile solutions (Table 1). However, even after such decrease, the TTF groups are too far away to allow any sizable through-space overlap between their orbitals. The charge distribution of the monomers in acetonitrile solutions is also similar to that on isolated monomers (Figure 3), as in both media the two highest occupied orbitals are the same. However, due to the smaller angle between the two L_i groups, the dipole moment of the monomers in solution is larger than when isolated (Table 1).

3.3.2. Solvent Effects on the $clip_2^{n+}$ Properties. The optimum geometries of $clip_2^{n+}$ (n < 6) dimers in acetonitrile solution (Figure S6, Supporting Information) are almost identical to their optimum isolated geometries (Figure 7). On the other hand, $clip_2^{6+}$ now preserves Figure 6c configuration, while $clip_2^{8+}$ presents a bound structure. Such similarity in n < 6 dimers is also manifested when the values of their most relevant interfragment geometrical parameters are examined (Table S4, Supporting Information). However, the charge distribution of $clip_2^{n+}$ dimers in solution (Figure 8) has two relevant differences with respect to the isolated dimer distribution: (a) the amount of positive charge on the TTF groups in

dx.doi.org/10.1021/ja405352p | J. Am. Chem. Soc. 2013, 135, 13814−13826

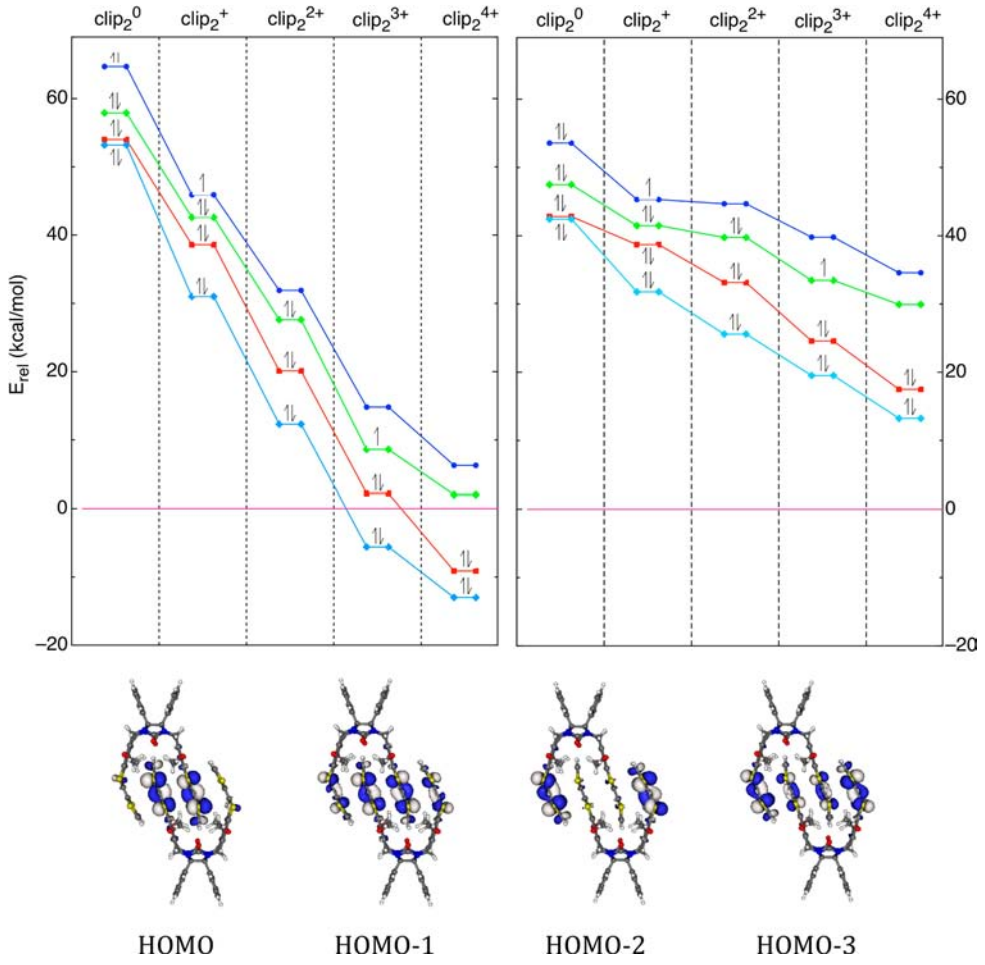

Figure 9. (top) Variation of orbital energy when $clip_2^0$ is oxidized to $clip_2^{n+}$ (n = 1−4), both isolated (left) and in acetonitrile (right). All results come from M06L/6-31G(d,p) calculations. In each dimer, its zero energy is the energy of the highest occupied orbital localized in L3/L4 groups. (bottom) Shape of the highest four occupied orbitals of an isolated $clip_2^0$ dimer (in acetonitrile solutions their shape is essentially the same).

acetonitrile (Table S6, Supporting Information) is remarkably larger than that in isolated dimers (Table S5, Supporting Information), and (b) the atomic charge becomes negligible in the two short arms. Those changes are associated with the different relative stability of the long and short arm orbitals in solution (Figure 9).

The formation energy of the dimers in acetonitrile solutions is collected in Table 2, together with their associated ΔG(298 K) values. The solvent destabilizes the formation of $clip_2^0$ and $clip_2^+$ dimers by 5 and 9 kcal/mol, respectively, but strongly stabilizes the formation of $clip_2^{2+}$, $clip_2^{3+}$, and $clip_2^{4+}$ (by 30, 63, and 140 kcal/mol, respectively). Therefore, according to the formation energies in acetonitrile, all $clip_2^{n+}$ $n \leq 6$ dimers are stable against their dissociation into monomers, and only the formation of the n = 8 dimer is slightly disfavored. Similar trends are found when looking at the values of ΔG(298 K) in acetonitrile, the property that better describes the behavior of the $clip_2^{n+}$ dimers under the experimental conditions. In perfect agreement with the reported experimental data, $clip_2^0$, $clip_2^+$, $clip_2^{2+}$, $clip_2^{3+}$, and $clip_2^{4+}$ are found to be more stable than their dissociated monomers, while $clip_2^{6+}$ and $clip_2^{8+}$ are metastable.

Such metastable character of $clip_2^{6+}$ and $clip_2^{8+}$ in acetonitrile was further evaluated by estimating whether the barrier for their dissociation into their constituting monomers is higher than the average thermal energy at 298 K (estimated as $T\Delta S$).[47] As seen in Figure S7, Supporting Information, at 298 K such barrier is smaller than the average thermal energy, thus allowing the dissociation of the dimer, in good agreement with the experimental data on the stability of $clip_2^{n+}$ dimers. In other words, solvent effects are essential for a proper reproducibility of the reported experimental stability of $clip_2^{n+}$ dimers.

The diagram in Figure 9 (right) also allows a proper rationalization of the available experimental UV−vis data on $clip_2^{n+}$ dimers in acetonitrile solutions. In $clip_2^+$ and $clip_2^{2+}$, Chiang et al.[25] obtained a low-energy band (~1650 nm). A higher energy band (~800 nm) was also obtained in $clip_2^{3+}$. In contraposition, $clip_2^{4+}$ only exhibits the higher energy band. Such behavior can be explained by considering the lowest two electronic energy transitions in these systems, which can be rationalized in terms of the MO diagram (identified in this analysis as HOMO, HOMO-1, HOMO-2, and HOMO-3), Figure 9. The lowest energy transition in $clip_2^+$ and $clip_2^{2+}$, which should be associated with the experimental ~1650 nm band, is the HOMO-1 → HOMO. In $clip_2^3$+ The HOMO-1 → HOMO transition is still the lowest one in energy, but a new transition, HOMO-2 → HOMO-1, is also possible, presumably responsible of the ~800 nm experimental band. In $clip_2^4$+ the HOMO-1 → HOMO cannot take place because the HOMO-1 orbital is empty. Consequently, the HOMO-2 → HOMO-1 transition becomes the lowest one in energy (and should be associated with the ~800 nm experimental band).

dx.doi.org/10.1021/ja405352p | J. Am. Chem. Soc. 2013, 135, 13814−13826

Table 3. Values of the Four Energy Components (in kcal/mol) of eq 2 Computed for the $clip_2^{n+}$ (n = 0, 1, 2, 3, 4, 6, or 8) Dimers[a]

	$E(2TTF_1-2TTF_2)$	$E(BR_1-BR_2)$	$E(2TTF_1-BR_2)$	$E(BR_1-2TTF_2)$	E_{sum}	E_{int}
$clip_2^{0}$	0/0	0/0	0/0	0/0		0/0
	−16.1	+0.01	−16.4	−16.4	−48.7	−49.5
$clip_2^{+}$	0/1+	0/0	0/0	0/1+		0/1+
	−28.5[b]	+0.01	−16.7[b]	−21.4[b]	−66.5	−64.2[b]
$clip_2^{2+}$	1+/1+	0/0	1+/0	0/1+		1+/1+
	+20.3	+0.01	−21.5	−21.5	−22.6	−25.5
$clip_2^{3+}$	1+/2+	0/0	1+/0	0/2+		1+/2+
	+56.7[b]	+0.01	−21.0[b]	−36.3[b]	−0.5	−2.7[b]
$clip_2^{4+}$	2+/2+	0/0	2+/0	0/2+		2+/2+
	+156.6	+0.01	−36.6	−36.6	+83.5	+80.9
$clip_2^{6+}$	3+/3+	0/0	3+/0	0/3+		3+/3+
	+264.7	+0.05	−75.3	−73.4	+116.1	+189.5
$clip_2^{8+}$	4+/4+	0/0	4+/0	0/4+		4+/4+
	+522.0	+0.05	−100.8	−103.8	+317.7	+370.5

[a]The following components were computed (see text for their definition): $2TTF_1-2TTF_2$, $2TTF_1-BR_2$, BR_1-2TTF_2, and BR_1-BR_2. The sum of these components (E_{sum}) is also given. In order to allow its easy comparison with the value of the BSSE-corrected interaction energy of the isolated dimer (E_{int}), this magnitude is also given (as extracted from the second row of Table 2). The charge on both interacting fragments is indicated in each box as fragment$_1$/fragment$_2$. All energy data are BSSE-corrected. [b]The system has two possible charge distributions, as 1+/0 or 0/1+, have been evaluated by calculating the average of both solutions.

3.4. The Origin of the Room Temperature Stability of the $clip_2^{n+}$ Dimers. As already mentioned, nonfunctionalized π-$[TTF]_2^{2+}$ dimers in acetonitrile solutions are experimentally found to be stable only up to −40 °C.[17] However, $clip_2^{4+}$ dimers dissolved in acetonitrile, which also have long $[TTF]^{\bullet+}\cdots[TTF]^{\bullet+}$ intradimer bonds, are experimentally detected at room temperature. Among other options, such a fact could be due to an increase in the stability of the long $[TTF]^{\bullet+}\cdots[TTF]^{\bullet+}$ intradimer bonds in $clip_2^{4+}$ dimers. This was investigated by doing a quantitative energy-partition analysis of the interaction energy of $clip_2^{n+}$, which also allowed to quantify the difference between the interaction energy of the long $[TTF]^{\bullet+}\cdots[TTF]^{\bullet+}$ intradimer bonds in π-$[TTF]_2^{2+}$ and $clip_2^{4+}$ dimers.

Before any other analysis, the interaction energy of the $[TTF]^{l+}\cdots[TTF]^{m+}$ interactions present in $clip_2^{n+}$ dimers was evaluated on isolated dimers. For such a task, in each $clip_2^{n+}$ dimer a $TTF_4(clip_2^{n+})$ aggregate was obtained by deleting all but the TTF groups,[48] and its total interaction energy, relative to two $TTF_2(clip_1^{m+})$ fragments, was computed (first column of Table 3). The difference between the interaction energy of the $TTF_4(clip_2^{n+})$ aggregate and the $clip_2^{n+}$ interaction energy relative to two $clip_1^{m+}$ fragments (last column of Table 3) manifestly suggests that the extra stability of $clip_2^{n+}$ dimers is caused by other than the $[TTF]^{l+}\cdots[TTF]^{m+}$ interactions. Such difference increases gradually from 33.4 kcal/mol in $clip_2^{0}$ to 151.5 kcal/mol in $clip_2^{8+}$, thus being significant even in the neutral $clip_2^{0}$.

The origin of the extra stability for the $clip_2^{n+}$ dimers was further investigated by breaking each monomer i in two parts: (a) the two TTF groups, $2TTF_i$, and (b) the rest, BR_i, which can be seen as a bridge connecting the two TTF groups of the monomer (Figure S9, Supporting Information). Within this partition scheme, the total interaction energy of a $clip_2^{n+}$ dimer is the sum of the following four components:

$$E_{int} \approx E(2TTF_1-2TTF_2) + E(2TTF_1-BR_2) + E(BR_1-2TTF_2) + E(BR_1-BR_2) \quad (2)$$

The values of these four terms for all $clip_2^{n+}$ dimers, computed at the optimum geometry of each dimer in acetonitrile, obtained at M06L/6-31G(d,p) level, are listed in Table 3. The validity of this partition scheme is demonstrated by noticing the similarity of the sum of these four terms (E_{sum}) and the total interaction energy (E_{int}).

It is also informative to look at the variation of the four components for the different $clip_2^{n+}$ dimers. First of all, $E(BR_1-BR_2)$ is very small in all dimers. Notice that although the bridge groups have a zero net charge, they have a strong dipole moment, originating in their zwitterionic charge distribution (Figure S10, Supporting Information). However, the large $BR_1\cdots BR_2$ intermolecular distance renders the E(dipole−dipole) and E_{disp} components zero (E_{bond} is also zero because, as already described, if any unpaired electron is present in the monomers, they are located in the TTF groups).

As previously stated, the $E(2TTF_1-2TTF_2)$ component accounts for the interaction between the TTF groups of each interacting fragment. Their disposition allows the existence of three face-to-face TTF···TTF interactions, two external and one internal. Since nearly all the positive charge gained by the dimer on its oxidation goes to its TTF groups, the changes in the $E(2TTF_1-2TTF_2)$ energetic component of $clip_2^{n+}$ (n = 0, 1, 2, 3, 4, 6, or 8) can be rationalized by looking at how the TTF···TTF interactions vary as the TTF groups get oxidized. Such information can be obtained from the properties of the π-$[TTF]_2^{n+}$ (n = 0−4) dimers.

M06L/6-31G(d,p) calculations were carried out on the π-$[TTF]_2^{n+}$ (n = 0−4) dimers (Figure S11, Supporting Information), checking their validity against extensive RASPT2/6-31G(d,p) calculations. The following conclusions were reached from these studies: (a) π-$[TTF]_2^{0}$ is a van der Waals dimer (where, $E_{int} \approx E_{disp}$, as E(charge−charge) = 0, because no net charge is present, and E_{bond} = 0, since there are no unpaired electrons) having a minimum 9.4 kcal/mol more stable than its dissociated fragments at an interfragment distance of about 3.45 Å; (b) π-$[TTF]_2^{+}$ has a stable dimer at an interfragment distance of 3.33 Å, whose energy is 20.4 kcal/mol more stable than that for its dissociated fragments

dx.doi.org/10.1021/ja405352p | J. Am. Chem. Soc. 2013, 135, 13814−13826

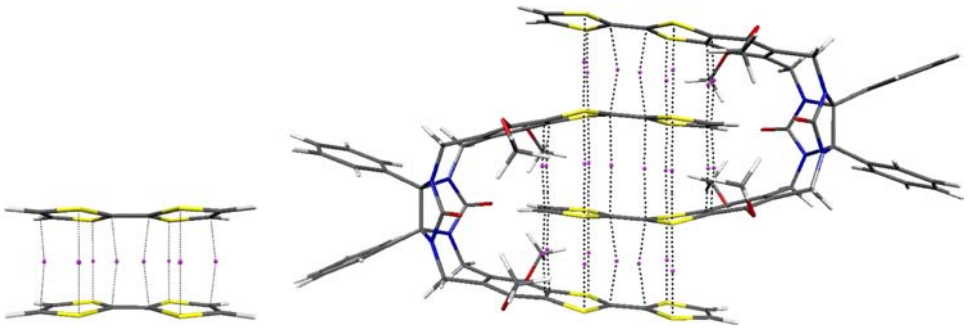

Figure 10. Position of the bond-critical points (purple) found between the $[TTF]^{\bullet+}$ groups in π-$[TTF]_2^{2+}$ (left) and in $clip_2^{4+}$ (right) at their optimum geometry in acetonitrile solution. Notice the similarity between the bond critical points in the external $[TTF]^{\bullet+}\cdots[TTF]^{\bullet+}$ interactions in $clip_2^{4+}$ and in π-$[TTF]_2^{2+}$. It is numerically demonstrated when the density in the critical points are compared, Table S7, Supporting Information.

(E_{bond} can be taken as zero, because there is only one unpaired electron and no pairing of electrons is possible, although much weaker one-electron bonds are also known; assuming that E_{disp} is dominated by the lone-pair···lone-pair interactions, one can expect that $E_{disp}(\pi\text{-}[TTF]_2^{0}) \approx E_{disp}(\pi\text{-}[TTF]_2^{+}) \approx E_{disp}(\pi\text{-}[TTF]_2^{2+})$; then, about half of the interaction energy would be due to E_{disp}, while the other half comes from the electrostatic component, thus allowing to classify this interaction as electrostatic dispersion, by looking at the dominant energetic components); (c) π-$[TTF]_2^{2+}$ is a long bonded dimer having a metastable minimum at about 3.44 Å whose energy is 38.1 kcal/mol above that of its dissociated fragments (its interaction energy is dominated by a repulsive E_{el} contribution, being the sum of the E_{disp} plus E_{bond} weaker, as usual in all known long bonded dimers;[7,8,10,11,13c,15] consequently, the $[TTF]^{\bullet+}\cdots[TTF]^{\bullet+}$ interaction is only produced in supramolecular aggregates due to the interaction of the $[TTF]^{\bullet+}$ groups with nearby counterions or solvent molecules);[10,19] and (d) π-$[TTF]_2^{3+}$ and π-$[TTF]_2^{4+}$ are unstable and show no bound minima along their dissociation potential energy curve (at a interfragment distance of 3.44 Å their interaction energy is 91 and 211 kcal/mol, respectively; the dominant energetic component is the electrostatic one, $E_{el} \approx E$(charge−charge), which becomes more repulsive than that in π-$[TTF]_2^{2+}$).

Given the relevance of the two long, multicenter bonds in $clip_2^{4+}$, its existence was subject of an in-depth analysis. Consistent with the considerations above, due to their shorter interfragment distance, in $clip_2^{4+}$ the SOMO($TTF^{\bullet+}$) + SOMO($TTF^{\bullet+}$) bonding combination of the two external $[TTF]^{\bullet+}\cdots[TTF]^{\bullet+}$ interactions is more stable than that for the internal interaction. Therefore, a long, multicenter bond is formed in each external $[TTF]^{\bullet+}\cdots[TTF]^{\bullet+}$ interaction, pairing the two unpaired electrons present in both $clip_1^{2+}$ fragments. As a consequence of their formation, no unpaired electrons remain in the dimer and the internal $[TTF]^{\bullet+}\cdots[TTF]^{\bullet+}$ interaction can only be a van der Waals interactions.[49] An atoms-in-molecules (AIM)[50,51] analysis of the π-$[TTF]_2^{2+}$ and $clip_2^{4+}$ electronic density confirms this rationalization (both densities were computed for the singlet ground state at their optimized geometry in acetonitrile solution). The results, graphically depicted in Figure 10, show the similar connectivity of the $[TTF]^{\bullet+}\cdots[TTF]^{\bullet+}$ bond critical points in both dimers. The same similarity is found in the bond critical point parameters (all bond critical points have densities within the 0.002 to 0.011 au range, see Table S7, Supporting Information). Finally, the strength of the long, multicenter bonds in $clip_2^{4+}$ and π-$[TTF]_2^{2+}$ is also similar: 24.2 kcal/mol (12.1 kcal/mol for each long bond)[52] in $clip_2^{4+}$ and 15.3 kcal/mol in π-$[TTF]_2^{2+}$. Therefore, the long, multicenter bonds in $clip_2^{4+}$ and π-$[TTF]_2^{2+}$ are similar, and thus, they cannot be the origin for the room temperature stability of $clip_2^{4+}$.

The last two terms in eq 2, $E(2TTF_1{-}BR_2)$ and $E(BR_1{-}2TTF_2)$, are both $[TTF]_2^{n+}\cdots$BR interactions. A detailed analysis of their geometry shows the presence of two interfragment C(sp^2)−H···O═C hydrogen bonds (the carbonyl located in the BR group, see Figure S9, Supporting Information) and four interfragment C(sp^3)−H···S hydrogen bonds (the C(sp^3)−H located in the BR group). It has been shown that, when both interacting fragments have a zero net charge, C(sp^2)−H···O═C and C(sp^3)−H···S hydrogen bonds are weaker than the O−H···O bonds found in a water dimer.[53] However, in all $clip_2^{n+}$ dimers a 1− au charge is located on the fused central rings (where the C═O groups are placed), while the n+ charge is spread over the two TTF groups of each $clip_1^{n+}$. Thus, both $E(2TTF_1{-}BR_2)$ and $E(BR_1{-}2TTF_2)$ terms are expected to be highly stabilizing since the two interacting fragments host charge of opposite sign (the existence of a net charge in fragments with proton donor and acceptor groups is known to enlarge the hydrogen bond strength, even beyond the 50 kcal/mol covalent limit).[54] Note that the simultaneous presence of two $E(2TTF_i{-}BR_j)$ interactions in each dimer is made possible by a proper design of the monomer geometry.

4. SUMMARY AND CONCLUSIONS

The reasons behind the existence of dimers of bis-TTF-functionalized diphenylglycoluril molecular clips ($clip_2^{n+}$) presenting short-distance $[TTF]^{l+}\cdots[TTF]^{m+}$ interactions, stable at room temperature when the dimer charge is ≤4, but not when $4 < n < 8$, have been investigated by computing their optimum geometry and analyzing their properties in detail. The computations were performed at the M06L/6-31G(d,p) level first on isolated dimers and then in dimers in acetonitrile solution, using the PCM model to describe the solvent effects.

All $clip_1^{m+}$ monomers present a V-shaped optimum geometry, where the distance between the two TTF groups placed at the end of each long arm increases about 2.0 Å (0.5 Å) from the neutral monomer to the tetraoxidized $clip_1^{4+}$ in isolated conditions (in solution). The optimum geometry of $clip_2^{n+}$ dimers consists of their two V-shaped interacting monomers oriented in opposite directions, where their long arms are intercalated, thus allowing the simultaneous formation of two types of short-distance intermolecular contacts: (a) three face-to-face TTF···TTF contacts between the adjacent TTF groups and (b) two C(sp^2)−H···O═C and four C(sp^3)−H···S

contacts between the TTF groups and the central fused five-membered rings. The values of $\Delta G(298\ K)$ computed for $clip_2^{n+}$ dimers in acetonitrile solutions reproduce the available experimental data on the stability of these dimers. Such agreement is not found when solvent effects are not taken into account.

The electronic structure of all monomers and the two interacting fragments in all dimers is similar and has a zwitterionic character: a 1− au of net charge is hosted on the central fused five-membered rings, while the net positive charge is mostly distributed on the two TTF groups, in an even way. Due to this fact, whenever all TTF groups of a $clip_2^{n+}$ dimer host a 1+ charge, as in $clip_2^{4+}$, two of the three short-distance face-to-face TTF···TTF contacts become long, multicenter $[TTF]^{\bullet+}\cdots[TTF]^{\bullet+}$ bonds, while the third one becomes a van der Waals interaction. As a result, the stability of these dimers increases.

An atoms-in-molecules analysis demonstrates that the long, multicenter bonds in $clip_2^{4+}$ and π-$[TTF]_2^{2+}$ are almost identical. Furthermore, the energy partitioning analysis shows that the $[TTF]^{l+}\cdots[TTF]^{m+}$ interactions themselves cannot be the origin for the room temperature stability of $clip_2^{n+}$ dimers. Instead, such energy partitioning analysis traces the four short-distance A−H···B contacts between the TTF and the fused five-membered rings to be the main force of the room temperature stability of $clip_2^{n+}$ dimers for $n \leq 4$. This fact is a consequence of the zwitterionic character of the charge distribution of the two interacting monomers of the dimer and their proper geometrical shape. Such geometrical arrangement also allows the formation of three short-distance contacts among the TTF groups, which eventually become long, multicenter bonds in $clip_2^{4+}$. All these factors, combined with the net stabilizing effect of the solvent, are outlined as the origin of the room temperature stability of $clip_2^{n+}$ dimers for $n \leq 4$.

■ ASSOCIATED CONTENT

Supporting Information

Basis set comparison, intramolecular parameters to define $clip_1^{n+}$ monomers in Table 1, charge distribution of $clip_1^{n+}$ monomers with several schemes, highest MOs of $clip_1^{n+}$ monomers, intermolecular parameters to define $clip_2^{n+}$ dimers, superimposed $clip_1^{n+}$ structures in gas phase and solution, optimum geometries of $clip_2^{n+}$ dimers in solution, scan of the PES in solution for the $clip_2^{4+}$, $clip_2^{6+}$, and $clip_2^{8+}$ dimers, fragment partition used in the fragment decomposition analysis, charge distribution in the bridge fragment, RASPT2/M06L comparison for isolated π-$[TTF]_2^{n+}$ dimers, intermolecular parameter values of $clip_2^{n+}$ dimers, distribution of the 1+ charge upon each subsequent oxidation, electron density at the bond critical points of $clip_2^{4+}$ and TTF_2^{2+}, Cartesian coordinates and absolute energies of all optimized species, and complete list of authors of ref 37. This material is available free of charge via the Internet at http://pubs.acs.org.

■ AUTHOR INFORMATION

Corresponding Author

juan.novoa@ub.edu

Notes

The authors declare no competing financial interest.

■ ACKNOWLEDGMENTS

We acknowledge the support given by the Ministry of Economic and Innovation of the Spanish Government, MINECO (Projects MAT2008-02032 and MAT2011-25972), a MINECO Ph.D. grant given to M.C., a University of Barcelona Ph.D. Grant given to M.F., and the support of the Catalan Autonomous Government (Grant 2009-SGR-1203). We also thank CESCA and BSC for their generous allocation of computer time in their machines. J.S.M. contributed to analysis of the results and appreciates the support by the Department of Energy Division of Material Science (No. DE-FG03-93ER45504), and U.S. National Science Foundation (No. 0553573).

■ REFERENCES

(1) Ferraro, J. R.; Williams, J. M. *Introduction to Synthetic Electrical Conductors*; Academic Press: Orlando, FL, 1987.

(2) Ishiguro, T.; Yamaji, K. *Organic Superconductors*; Spinger-Verlag: Berlin, 1990.

(3) (a) Kahn, O. *Molecular Magnetism*; VCH: New York, 1993. (b) Miller, J. S.; Epstein, A. *Angew. Chem., Int.. Ed.* **1994**, *33*, 385. (c) Lahti, P. M., Ed. *Magnetic Properties of Organic Materials*; Marcel Dekker: New York, 1999. (d) Itoh, K.; Kinoshita, M. *Molecular Magnetism: New Magnetic Materials*; Kodansha: Tokyo, 2000. (e) Veciana, J. *π-Electron Magnetism. From Molecules to Magnetic Materials*; Springer: Berlin, 2001. (f) Miller, J. S.; Drillon, Eds. *Magnetism: Molecules to Devices V*; Wiley-VCH: Weinheim, Germany, 2006.

(4) Novoa, J.; Braga, D.; Addadi, L., Eds. *Engineering of Crystalline Materials Properties*; Springer: Dordrecht, the Netherlands, 2007.

(5) Nielsen, M. B.; Lomholt, C.; Becher, J. *Chem. Soc. Rev.* **2000**, *29*, 153.

(6) (a) Hasegawa, T.; Mattenberger, K.; Takeya, J.; Batlogg, B. *Phys. Rev. B* **2004**, *69*, No. 245115. (b) Sakai, M.; Sakuma, H.; Ito, Y.; Saito, A.; Nakamura, M.; Kudo, K. *Phys. Rev. B* **2007**, *76*, No. 045111. (c) Takahashi, Y.; Hasegawa, T.; Abe, Y.; Tokura, Y.; Nishimura, K.; Saito, G. *Appl. Phys. Lett.* **2005**, *86*, No. 063504. (d) Takahashi, Y.; Hasegawa, T.; Abe, Y.; Tokura, Y.; Saito, G. *Appl. Phys. Lett.* **2006**, *88*, No. 073504. (e) Zhu, L.; Yi, Y.; Li, Y.; Kim, E.-G.; Coropceanu, V.; Brédas, J.-L. *J. Am. Chem. Soc.* **2012**, *134*, 2340.

(7) (a) Novoa, J. J.; Lafuente, P.; Del Sesto, R. E.; Miller, J. S. *Angew. Chem., Int. Ed.* **2001**, *40*, 2540. (b) Del Sesto, R. E.; Miller, J. S.; Lafuente, P.; Novoa, J. J. *Chem.—Eur. J.* **2002**, *8*, 4894. (c) Novoa, J. J.; Lafuente, P.; Del Sesto, R. E.; Miller, J. S. *CrystEngComm* **2002**, *4*, 373. (d) Tian, Y.-H.; Kertesz, M. *J. Phys. Chem. A* **2011**, *115*, 13942.

(8) Miller, J. S.; Novoa, J. J. *Acc. Chem. Res.* **2007**, *40*, 189.

(9) Lü, J.-M.; Rosokha, S. V.; Kochi, J. K. *J. Am. Chem. Soc.* **2003**, *125*, 12161.

(10) Garcia-Yoldi, I.; Mota, F.; Novoa, J. J. *J. Comput. Chem.* **2007**, *28*, 326.

(11) Garcia-Yoldi, I.; Miller, J. S.; Novoa, J. J. *Phys. Chem. Chem. Phys.* **2008**, *10*, 4106.

(12) (a) Reis, A. H., Jr.; Gebert, E.; Miller, J. S. *Inorg. Chem.* **1981**, *20*, 313. (b) Goldberg, S. Z.; Spivack, B.; Stanley, G.; Eisenberg, R.; Braitsch, D. M.; Miller, J. S.; Abkowitz, M. *J. Am. Chem. Soc.* **1977**, *99*, 110. (c) Grossel, M. C.; Evans, F. A.; Hriljac, J. A.; Prout, K.; Weston, S. C. *J. Chem. Soc., Chem. Commun.* **1990**, 1494. (d) Axcondo, M. T.; Ballester, J.; Golhen, S.; Gutierrez, A.; Ouahab, L.; Yartsev, S.; Delhaes, P. *J. Mater. Chem.* **1999**, *9*, 1237. (e) Hynes, R. C.; Morton, J. R.; Preston, K. F.; Williams, A. J.; Evans, F.; Grossel, M. C.; Sutcliffe, L. H.; Weston, S. C. *J. Chem. Soc., Faraday Trans.* **1991**, *87*, 2229. (f) Miller, J. S.; Zhang, J. H.; Reiff, W. M.; Preston, L. D.; Reis, A. H., Jr.; Gerbert, E.; Extine, M.; Troup, J.; Ward, M. D. *J. Phys. Chem.* **1987**, *91*, 4344. (g) Garcia-Yoldi, I.; Miller, J. S.; Novoa, J. J. *J. Phys. Chem. A* **2009**, *113*, 7124.

(13) (a) Goto, G.; Kubo, T.; Yamamoto, K.; Nakazawa, S. K.; Sato, K.; Shiomi, D.; Takui, T.; Kubota, M.; Kobayshai, Y.; Yakusi, K.;

Ouyang, J. A. *J. Am. Chem. Soc.* **1999**, *121*, 1619. (b) Small, D.; Zaitsev, V.; Jung, Y.; Rosokha, S. V.; Head-Gordon, M.; Kochi, J. K. *J. Am. Chem. Soc.* **2004**, *126*, 13850. (c) Mota, F.; Miller, J. S.; Novoa, J. J. *J. Am. Chem. Soc.* **2009**, *131*, 7699.

(14) (a) Torrance, J. B.; Scott, B. A.; Welber, B.; Kaufman, F. B.; Seiden, P. E. *Phys. Rev. B* **1979**, *19*, 730. (b) Yakushi, K.; Nishimura, S.; Sugano, T.; Kuroda, H. *Acta Crystallogr.* **1980**, *B36*, 358. (c) Sugano, T.; Kuroda, H.; Yakushi, K. *Bull. Chem. Soc. Jpn.* **1978**, *51*, 1041. (d) Yamashita, A.; Akutsu, H.; Yamada, J.; Nakatsuji, S. *Polyhedron* **2005**, *24*, 2796. (e) Matsubayashi, G.; Ueyama, K.; Tanaka, T. *J. Chem. Soc., Dalton Trans.* **1985**, 465. (f) Furuta, K.; Akutsu, H.; Yamada, J.; Nakatsuji, S. *Synth. Met.* **2005**, *152*, 381. (g) Morgado, J.; Santos, I. C.; Veiros, L. F.; Rodrigues, C.; Henriques, R. T.; Duarte, M. T.; Alcacer, L.; Almeida, M. *J. Mater. Chem.* **2001**, *11*, 2108. (h) Libage, C.; Fourmigue, M.; Batail, P.; Canadell, E.; Coulon, C. *Bull. Soc. Chim. Fr.* **1993**, *130*, 761. (i) Yamochi, H.; Konsha, A.; Saito, G.; Matsumoto, K.; Kusunoki, M.; Sakaguchi, K. *Mol. Cryst. Liq. Cryst. Sci. Technol., Sect. A* **2001**, *350*, 265. (j) Akutsu, H.; Masaki, M.; Mori, K.; Yamada, J.; Nakatsuji, S. *Polyhedron* **2005**, *24*, 2126. (k) Giffard, M.; Mabon, G.; Leclair, E.; Mercier, N.; Allain, M.; Gorgues, A.; Molinie, P.; Neilands, O.; Krief, P.; Khodorkowsky, V. *J. Am. Chem. Soc.* **2001**, *123*, 3852. (l) Slougui, A.; Ouahab, L.; Perrin, C.; Grandjean, D.; Batail, P. *Acta Crystallogr.* **1989**, *C45*, 388. (m) Teitelbaum, R. C.; Marks, T. J.; Johnson, C. K. *J. Am. Chem. Soc.* **1980**, *102*, 2986. (n) Coronado, E.; Galan-Mascaros, J. R.; Gimenez-Sais, C.; Gomez-Garcia, C. J.; Ruiz-Perez, C.; Triki, S. *Adv. Mater.* **1996**, *8*, 737.

(15) Garcia-Yoldi, I.; Miller, J .S.; Novoa, J. J. *J. Phys. Chem. A* **2009**, *113*, 484.

(16) Capdevila-Cortada, M.; Novoa, J. J.; Bell, J. D.; Moore, C. E.; Rheingold, A. L.; Miller, J. S. *Chem.—Eur. J.* **2011**, *17*, 9326.

(17) Rosokha, S. V.; Kochi, J. K. *J. Am. Chem. Soc.* **2007**, *129*, 828.

(18) Jakowski, J.; Simons, J. *J. Am. Chem. Soc.* **2003**, *125*, 16089.

(19) Jung, Y.; Head-Gordon, M. *Phys. Chem. Chem. Phys.* **2004**, *6*, 2008.

(20) (a) Spruell, J. M.; Coskun, A.; Friedman, D. C.; Forgan, R. S.; Sarjeant, A. A.; Trabolsi, A.; Fahrenbach, A. C.; Barin, G.; Paxton, W. F.; Dey, S. K.; Olson, M. A.; Benitez, D.; Tkatchouk, E.; Colvin, M. T.; Carmielli, R.; Caldwell, S. T.; Rosair, G. M.; Hewage, S. G.; Duclairoir, F.; Seymour, J. L.; Slawin, A. M. Z.; Goddard, W. A., III; Wasielewski, M. R.; Cooke, G.; Stoddart, J. F. *Nat. Chem.* **2010**, *2*, 870. (b) Coskun, A.; Spruell, J. M.; Barin, G.; Fahrenbach, A. C.; Forgan, R. S.; Colvin, M. T.; Carmieli, R.; Benítez, D.; Tkatchouk, E.; Friedman, D. C.; Sarjeant, A. A.; Wasielewski, M. R.; Goddard, W. A., III; Stoddart, J. F. *J. Am. Chem. Soc.* **2011**, *133*, 4538.

(21) Capdevila-Cortada, M.; Novoa, J. J. *Chem.—Eur. J.* **2012**, *18*, 5335.

(22) Ziganshina, A. Y.; Ko, Y. H.; Jeon, W. S.; Kim, K. *Chem. Commun.* **2004**, 806.

(23) Jeon, W. S.; Kim, H.-J.; Lee, C.; Kim, K. *Chem. Commun.* **2002**, 1828.

(24) Lyskawa, J.; Salle, M.; Balandier, J. Y.; Le Derf, F.; Levillain, E.; Allain, M.; Viel, P.; Palacin, S. *Chem. Commun.* **2006**, 2233.

(25) Chiang, P. T.; Chen, N. C.; Lai, C. C.; Chiu, S. H. *Chem.—Eur. J.* **2008**, *14*, 6546.

(26) Miertus, S.; Scrocco, E.; Tomasi, J. *Chem. Phys.* **1981**, *55*, 117.

(27) Fuoss, R. M. *J. Am. Chem. Soc.* **1958**, *80*, 5059.

(28) Zhao, Y.; Truhlar, D. G. *Theor. Chem. Acc.* **2008**, *120*, 215.

(29) Dietchfield, R.; Hehre, W. J.; Pople, J. A. *J. Chem. Phys.* **1971**, *54*, 724.

(30) Risthaus, T.; Grimme, S. *J. Chem. Theory Comput.* **2013**, *9*, 1580.

(31) Malmqvist, P.-A.; Pierloot., K.; Moughal Shahi, A. R.; Cramer, C. J.; Gagliardi, L. *J. Chem. Phys.* **2008**, *128*, 204109.

(32) RASPT2, a second-order Moller−Plesset computation based on a restricted active space wave function, is a variety of CASPT2 computation where the CAS space is divided into three subspaces, RAS1, RAS2, and RAS3, and only certain excitations are allowed between the RAS1 and RAS3 spaces, while all excitations are allowed in the RAS2 subspace.

(33) The active space is defined as follows: number of electrons in all RAS space, maximum number of holes in RAS1, maximum number of particles in RAS3; orbitals in RAS1, orbitals in RAS2, orbitals in RAS3.

(34) Pou-Amérigo, R.; Orti, E.; Merchán, M.; Rubio, M.; Viruela, P. *J. Phys. Chem. A* **2002**, *106*, 631.

(35) Boys, S. F.; Bernardi, F. *Mol. Phys.* **1970**, *19*, 553.

(36) For a numerical demonstration of the performance on ab initio methods of the counterpoise method as the basis set increases, see: (a) Novoa, J. J.; Planas, M.; Whangbo, M.-H. *Chem. Phys. Lett.* **1994**, *225*, 240. (b) Novoa, J. J.; Planas, M.; Rovira, C. *Chem. Phys. Lett.* **1996**, *251*, 33. (c) Novoa, J. J.; Sosa, C. *J. Phys. Chem.* **1995**, *99*, 15837.

(37) Frisch, M. J.; et al. *Gaussian 09*, revision C.1; Gaussian, Inc.: Wallingford CT, 2009.

(38) Aquilante, F.; De Vico, L.; Ferré, N.; Ghigo, G.; Malmqvist, P.-Å.; Neogrády, P.; Pedersen, T. B.; Pitonak, M.; Reiher, M.; Roos, B. O.; Serrano-Andrés, L.; Urban, M.; Veryazov, V.; Lindh, R. *J. Comput. Chem.* **2010**, *31*, 224.

(39) Zwitterions are defined as neutral compounds having formal electrical charges of opposite sign in different regions of their structure. See IUPAC.. *Compendium of Chemical Terminology*, 2nd ed. (the"Gold Book"); Compiled by McNaught, , A. D.; Wilkinson, , A.; Blackwell Scientific Publications: Oxford, **1997**,.

(40) The dipole moment of an isolated water monomer is 1.855 D. Lovas, D. F. J. *J. Phys. Chem. Ref. Data* **1978**, *7*, 1445.

(41) Hayes, I. C.; Stone, A. J. *J. Mol. Phys.* **1984**, *53*, 83.

(42) (a) Rigby, M.; Smith, E. B.; Wakeham, W. A.; Maitland, G. C. *The Forces between Molecules*; OUP: Oxford, 1986. (b) Stone, A. J. *The Theory of Intermolecular Forces*; OUP: Oxford, 1997.

(43) When $n = 0$, $E_{el} \approx E$(dipole−dipole). When $n > 0$, a repulsive E(charge−charge) term is also present in E_{el}. As n increases, the $clip_1^{n+}$ dipole moment increases and so does E(dipole−dipole). But simultaneously the repulsive E(charge−charge) term becomes more repulsive. It is difficult to estimate the net sign of E_{int} in all $clip_2^{m+}$ dimers, but it gives an explanation about why $clip_2^{m+}$ dimers are not detected experimentally when $m = 2n > 4$.

(44) Besides $clip_2^{2+}$ and $clip_2^{4+}$, in an increasing order of net charge in the $clip_2^{n+}$ dimer, (1) $clip_2^{+}$ is a $clip_1^{+}\cdots clip_1^{0}$ interaction presenting one three-electron $[TTF]^{\bullet+}\cdots[TTF]$ interaction and one $[TTF]\cdots[TTF]$ closed-shell interaction, (2) $clip_2^{3+}$ is a $clip_1^{2+}\cdots clip_1^{+}$ interaction presenting one $[TTF]^{\bullet+}\cdots[TTF]^{+}$ long bond interaction and one three-electron $[TTF]^{\bullet}\cdot\cdot[TTF]^{\bullet+}$ interaction; (3) $clip_2^{5+}$ is a $clip_1^{3+}\cdots clip_1^{2+}$ interaction presenting one one-electron $[TTF]^{2+}\cdots[TTF]^{\bullet+}$ interaction and one $[TTF]^{\bullet+}\cdots[TTF]^{\bullet+}$ long bond interaction; (4) $clip_2^{6+}$ is a $clip_1^{3+}\cdots clip_1^{3+}$ interaction presenting two one-electron interactions, $[TTF]^{2+}\cdots[TTF]^{\bullet+}$ and $[TTF]^{\bullet+}\cdots[TTF]^{2+}$; and (5) $clip_2^{8+}$ is a $clip_1^{4+}\cdots clip_1^{4+}$ interaction presenting two closed-shell $[TTF]^{2+}\cdots[TTF]^{2+}$ interactions, so no long bonds can be formed in this case.

(45) A detailed quantitative analysis of the optimum geometry of all dimers was done, comparing the values of the intermolecular parameters defined in Figure S4, Supporting Information. The results (Table S1, Supporting Information) confirmed the similar geometrical disposition of the fragment in all dimers. The two TTF groups from one monomer are interlocked with those of the other, forming a four-membered π-stack. Depending on the net charge of the TTF groups, their relative disposition varies from a fully oblique conformation (similar to that found in isolated $[TTF]_2^{0}$ and $[TTF]_2^{+}$ dimers, see Figure S2, Supporting Information) into an on-top disposition (as in the optimum structure of isolated $[TTF]_2^{2+}$, Figure S2, Supporting Information). Also relevant is the presence of short C−H···O intermolecular contact (d_2(O−H)) between the terminal TTF of one fragment and the C═O bond of the central ring of the other. When the clip hosting the C−H group is oxidized, the TTF group get the extra positive charge, while the CR group where the C═O is located hosts a 1− net charge. These are the conditions for a very strong ion···ion hydrogen bond, see: D'Oria, E.; Novoa, J. J. *J. Phys. Chem. A* **2011**, *115*, 13114.

(46) By metastable minimum, we refer here to fully characterized minima in the potential energy surface whose energy is higher than

that for their dissociation fragments, but where the existence of a barrier towards dissociation prevents such a dissociation process.
(47) The barriers were estimated as follows: (1) the potential energy curve for the separation of the dimer into their monomers in solution was computed, after freezing the monomer geometries at their value in the dimer structure; (2) the geometry of the highest energy point was fully optimized, fixing only the monomer separation.
(48) The two C−C bonds that connect them to the rest of the clip were substituted by C−H bonds, the H atoms oriented along the same direction than the C-C bonds, but placed at a C−H distance of 1.07 Å.
(49) Consistent with this view, the external $[TTF]^{\bullet+}\cdots[TTF]^{\bullet+}$ interactions present a geometry close to the usual one in π-$[TTF]_2^{2+}$ dimers, which present long, multicenter bonds, while the internal $[TTF]^{\bullet+}\cdots[TTF]^{\bullet+}$ interaction present a distance similar to that found in π-$[TTF]_2^{0}$ dimers, a van der Waals dimer.
(50) Bader, R. F. W. *Atoms in Molecules. A Quantum Theory*; Clarendon Press: Oxford, 1990.
(51) The analysis was done using an in-house version of the PROAIMS program.
(52) It can be taken as the energy required to break the two long bonds, that is, E(long-bond) = [E(Q-clip$_2^{4+}$) − E(S-clip$_2^{4+}$)]
(53) (a) Novoa, J. J.; Tarrón, B.; Whangbo, M.-H.; Williams, J. M. *J. Chem. Phys.* **1991**, *95*, 5179. (b) Novoa, J. J.; Constans, P.; Whangbo, M.-H. *Angew. Chem., Int. Ed. Engl.* **1993**, *32*, 588. (c) Novoa, J. J.; Rovira, C.; Rovira, C.; Veciana, J.; Tarres, J. *Adv. Mater.* **1995**, *7*, 233. (d) Novoa, J. J.; Mota, F. *Chem. Phys. Lett.* **1997**, *266*, 23. (e) Novoa, J. J.; Lafuente, P.; Mota, F. *Chem. Phys. Lett.* **1998**, *290*, 519. (f) Novoa, J. J.; Mota, F.; D'Oria, E. The nature of the C-H...X intermolecular interactions in molecular crystals. A theoretical perspective. In *Hydrogen bonding − New insights*; Grabowski, S., Ed.; Springer: Dordrecht, the Netherlands, 2006; Chapter 5, pp 193−244. (h) Braga, D.; Grepioni, F.; Novoa, J. J. *Chem. Commun.* **1998**, 1959. (i) D'Oria, E.; Novoa, J. J. *CrystEngComm* **2004**, *6*, 367. (j) D'Oria, E.; Novoa, J. J. *J. Phys. Chem. A* **2011**, *115*, 13114.
(54) (a) Novoa, J. J.; Tarrón, B.; Whangbo, M.-H.; Williams, J. M. *J. Am. Chem. Soc.* **1991**, *113*, 9017. (b) Novoa, J. J.; Constans, P.; Whangbo, M.-H. *Angew. Chem., Int. Ed. Engl.* **1993**, *32*, 588. (c) Braga, D.; Grepioni, F.; Novoa, J. J. *Chem. Commun.* **1998**, 1959. (d) Novoa, J. J.; Mota, F.; D'Oria, E. The nature of the C-H...X intermolecular interactions in molecular crystals. A theoretical perspective. In *Hydrogen bonding − New insights*; Grabowski, S., Ed.; Springer: Dordrecht, the Netherlands, 2006; Chapter 5, pp 193−244